Bioresource Technology 102 (2011) 416–421

Contents lists available at ScienceDirect

Bioresource Technology

journal homepage: www.elsevier.com/locate/biortech

Time-course correlation of biofilm properties and electrochemical performance in single-chamber microbial fuel cells

Zhiyong Ren [a,c], Ramaraja P. Ramasamy [b,1], Susan Red Cloud-Owen [b], Hengjing Yan [a], Matthew M. Mench [b], John M. Regan [a,*]

[a] Department of Civil and Environmental Engineering, The Pennsylvania State University, University Park, PA 16802, USA
[b] Department of Mechanical and Nuclear Engineering, The Pennsylvania State University, University Park, PA 16802, USA
[c] Department of Civil Engineering, University of Colorado Denver, Denver, Colorado 80217, USA

ARTICLE INFO

Article history:
Received 14 March 2010
Received in revised form 1 June 2010
Accepted 2 June 2010
Available online 29 June 2010

Keywords:
Microbial fuel cell
Electricity
Biofilm
Electrochemical impedance spectroscopy

ABSTRACT

The relationship between anode microbial characteristics and electrochemical parameters in microbial fuel cells (MFCs) was analyzed by time-course sampling of parallel single-bottle MFCs operated under identical conditions. While voltage stabilized within 4 days, anode biofilms continued growing during the six-week operation. Viable cell density increased asymptotically, but membrane-compromised cells accumulated steadily from only 9% of total cells on day 3 to 52% at 6 weeks. Electrochemical performance followed the viable cell trend, with a positive correlation for power density and an inverse correlation for anode charge transfer resistance. The biofilm architecture shifted from rod-shaped, dispersed cells to more filamentous structures, with the continuous detection of *Geobacter sulfurreducens*-like 16S rRNA fragments throughout operation and the emergence of a community member related to a known phenazine-producing *Pseudomonas* species. A drop in cathode open circuit potential between weeks two and three suggested that uncontrolled biofilm growth on the cathode deleteriously affects system performance.

1. Introduction

Microbial fuel cells (MFCs) employ microorganisms as biocatalysts to directly convert biodegradable substrates into electricity. The variable biocatalyst density (or electrochemically active volume of the anode biofilm) associated with microbial growth and decay is a unique feature of MFCs relative to traditional electrochemical fuel cells with metal catalysts (Mench, 2008) or enzyme-based biofuel cells (Kim et al., 2006), which only have an initial catalyst loading and subsequent catalyst decay. However, the effect of this factor on system performance was shadowed by the high internal resistances in early MFC designs. Improvements of MFC architecture have significantly relieved the physical, chemical, and ohmic constraints to power production, which opens the door to explore and address the microbial kinetic constraints of MFCs (Logan and Regan, 2006).

Most studies operate MFCs at fixed external resistances or applied potentials, allow the systems to reach an apparent steady state based on voltage or current profiles, and then compare system performance based on polarization and power density curves (Logan et al., 2006). These collective MFC data have had little or no regard to the time-varying biocatalyst density and changes in this potentially performance-limiting attribute under microbially meaningful timescales. With known mechanisms of anode reduction from cells that are not immediately adjacent to the anode (Gorby et al., 2006; Rabaey et al., 2005; Reguera et al., 2005), the effective biocatalyst availability should increase with biofilm density until mass transfer limitations develop in terms of both substrate transport and electron conductance within thicker or denser biofilms, so that a peak performance should exist. It has been demonstrated that the anode electrochemical polarization resistance can constrain system performance in both two-chamber and single-chamber MFCs (Ramasamy et al., 2008b,c). Moreover, microbial biofilm growth of either mixed culture or *Shewanella oneidensis* MR-1 decreased the anode polarization resistance significantly and facilitated the kinetics of the electrochemical reactions, presumably due to an increase in biocatalyst density as well as an increase in the quantity of endogenously produced metabolites that may assist in extracellular electron transfer (Manohar et al., 2008; Ramasamy et al., 2008c). Similar trends were found in continuous running stack MFCs, where the internal resistance of the MFCs decreased over time, accompanied by the growth and community change of microbial biofilm and increase of power output

* Corresponding author. Tel.: +1 814 865 9436.
E-mail address: jregan@engr.psu.edu (J.M. Regan).
[1] Present address: Airbase Sciences Branch RXQL, U.S. Air Force Research Laboratory, Tyndall AFB, FL 32403, USA.

0960-8524/$ - see front matter © 2010 Elsevier Ltd. All rights reserved.
doi:10.1016/j.biortech.2010.06.003

(Aelterman et al., 2006). However, to our knowledge no study has yet directly demonstrated how biofilm growth correlates with electrochemical performance in MFCs.

Since the sustainable microbially induced current density can be one of the major limitations to power production in MFCs, increasing and maintaining biocatalyst density presents a prime opportunity to continue the dramatic improvements in MFC performance. The aim of this study is to investigate the time-course correlation of biofilm growth, anode kinetics, and system performance and therefore provide insight into electrochemical constraints, the influence of biofilm architecture and composition on these constraints, and approaches to maintain a more electro-catalytically productive anode biofilm.

2. Methods

2.1. MFC construction

Six single-chamber bottle-type MFCs used in this study were modified from B-MFCs (Logan et al., 2007) by using Wheaton graduated media bottles (250 mL, Wheaton, NJ) and rubber-top lined caps to provide an air-tight condition. The anodes were made of plain carbon paper (BASF, NJ, projected area of 19.5 cm^2, two sides), and air cathodes (projected area of 4.5 cm^2, one side) were made by applying Pt/C (0.5 mg/cm^2) and four PTFE diffusion layers on 30% wet-proofed carbon cloth (BASF) as previously described (Cheng et al., 2006). The anode and cathode were connected to 1000 Ω external resistors. Reference electrodes (RE-5B, Bioanalytical Systems Inc., OH) were introduced into the anode chamber for conducting electrochemical measurements on individual electrodes.

2.2. Culture inoculation and reactor operation

MFCs were inoculated using anaerobic sludge obtained from the Pennsylvania State University Wastewater Treatment Plant. The reactors were fed with 250 mL medium containing 1.0 g/L of sodium acetate, 0.31 g/L of NH_4Cl, 0.13 g/L of KCl, 5.85 g/L of $NaH_2PO_4{\cdot}H_2O$, 4.09 g/L of Na_2HPO_4, 12.5 mL/L of mineral solution, and 12.5 mL/L of vitamin solution (Ren et al., 2007b). The medium was adjusted to pH 7.0, autoclaved, and cooled before the addition of filter-sterilized mineral and vitamin solutions. All MFCs were operated in fed-batch mode at 30 °C, and sterile medium was replaced every week before observing a voltage drop associated with substrate depletion.

2.3. Electrochemical analyses

Cell voltage was continuously monitored using a data acquisition system (Keithley Instruments, OH). A reactor was randomly selected for electrochemical and microbial analyses at day 3, day 7 (1 week), day 14 (2 weeks), and day 21 (3 weeks), and the two remaining reactors were sampled after 6 weeks for replicate electrochemical analyses. After operating each reactor for its respective duration, it was removed from routine operation and polarization and electrochemical impedance spectroscopy (EIS) tests (He and Mansfeld, 2009) were performed using a Zahner™ IM6ex potentiostat-AC frequency analyzer. The results were analyzed using Thales® software. Impedance measurements were taken on three configurations designated full cell (FC), anode (A), and cathode (C), and the impedance data were fitted to the equivalent electrical circuit as previously described (Ramasamy et al., 2008a; Ramasamy et al., 2008c) to obtain key parameters such as electrochemical charge transfer resistance for the anode and the cathode. The frequency of the AC signal was varied from 10 kHz to 100 mHz with an amplitude of ±10 mV. Impedance experiments were performed under galvanostatic closed-circuit conditions at 25 and 250 mA/m^2, which were estimated from the polarization data to represent the bounds of the kinetic impedance for this reactor setup. To ensure steady state during galvanostatic operation, the MFCs were allowed to equilibrate for 10 min before applying the AC signal.

2.4. Anode biofilm analyses

Each MFC was disassembled after EIS analyses for anode biofilm observation and community characterization. A section of anode was mounted onto a glass slide with an edge support that had the same thickness as the carbon paper to allow a cover slip to rest above the biofilm (Ren et al., 2008). The biofilm was then stained for 15 min using the LIVE/DEAD® BacLight™ Bacterial Viability Kit (Invitrogen, CA), which assays membrane integrity, and mounted in DABCO to reduce photo-bleaching. Visualization of the stained anode biofilm was performed on an Olympus Fluoview 1000 Confocal Laser Scanning Microscope (CLSM; Olympus America Inc., NY). The three-dimensional biofilm architecture (z-stack) was scanned and displayed as an ortho view. Images were analyzed by Photoshop and FV10-ASW software.

Biofilm cell counts were performed by destructing 1 cm^2 anode using a sterilized scissor in a 2 ml centrifuge tube with 50 mM phosphate buffer, followed by separating microbial biomass from carbon fibers through gentle vortexing and then short slow-speed centrifugation (5000 rpm, 1 min). This detachment method was used to avoid effects on membrane integrity. Suspended cells were serially diluted and stained using the viability staining kit, filtered through a 0.45 μm membrane filter, and counted using a Zeiss Axiophot epifluorescent microscope. The cell density per anode geometric area was calculated using the dilution factor, the filtered volume, and the ratio of total filtered area to image area. Some samples were also counterstained using 4′-6-diamidino-2-phenylindole (DAPI) for comparison.

The phylogenetic composition of anode biofilm communities was determined by 16S rRNA gene-targeted PCR, denaturing gradient gel electrophoresis (DGGE) screening of PCR products, cloning and sequencing of prominent DGGE bands, and phylogenetic analysis. Carbon paper anode subsamples were cut and fragmented using sterile razors, and genomic DNA was extracted using the PowerSoil™ DNA Isolation Kit (MO BIO Laboratories Inc., Carlsbad, CA) according to the manufacturer's instructions. A fragment of the 16S rRNA gene was PCR amplified using a pair of universal primers: 968F 5′-AACGCGAAGAACCTTAC-3′ (*E. coli* 16S rRNA positions 968–984) to which was attached a GC clamp (CGCCCGCCGC GCCCCGCGCCCGTCCCGCCGCCCCCGCCCG) at the 5′-terminus, and 1401R, 5′-CGGTGTGTACAAGACCC -3′ (*E. coli* 16S rRNA gene positions 1385–1401) (Ren et al., 2007a). PCR amplification was carried out in 25-μl volumes containing 12.5 μl of Master Mix (QIAGEN, Valencia, CA), 0.5 μM of each primer, 5 μl of DNA extraction, and water. The samples were amplified in an iCycler iQ™ (Bio-Rad Laboratories, Hercules, CA) with an initial denaturation of DNA for 4 min at 95 °C; 35 cycles of 30 s at 95 °C, 30 s at 60 °C (decreasing 0.1 °C per cycle to 58 °C), and 1 min at 72 °C; and final extension for 7 min at 72 °C. Blank controls were carried out through all steps.

DGGE was performed with a DCode universal mutation detection system (Bio-Rad Laboratories, Hercules, CA). Approximately 1 μg of PCR products per lane were loaded onto 7% (wt/vol) polyacrylamide (37.5:1 acrylamide: bisacrylamide) gels in a 1X TAE buffer with a denaturing gradient ranging from 30–60%. Denaturation of 100% corresponds to 7 M urea and 40% (vol/vol) deionized formamide. Electrophoresis was run for 10 min at 30 V and 12 h at 70 V in 1X TAE buffer maintained at 60 °C. Gels were silver stained as previously described (Bassam et al., 1991). Prominent DGGE bands were excised, and the gel was crushed in 50 μl TE buffer

and allowed to equilibrate overnight at 4 °C. Then 3 μl of buffer containing DNA was used as the template for a PCR performed under the conditions described above, except that the forward primer lacked the GC clamp. PCR products were purified using a QIAquick Gel Extraction Kit (QIAGEN, Valencia, CA), ligated into vector pCR2.1 using a TOPO TA cloning kit (Invitrogen, Carlsbad, CA), and cloned into chemically competent One Shot *Escherichia coli* cells provided with the cloning kit, as recommended by the manufacturer's instructions. Plasmids were isolated with the E-Z 96 Fastfilter Plasmid Kit (Omega Bio-Tek, Norcross, GA) from five randomly selected clone colonies for each band, and the inserts were sequenced (ABI 3730XL DNA sequencer, Applied Biosystems, Foster, CA) to determine whether multiple 16S rRNA fragments had co-migrating on the DGGE band. The 16S rRNA gene sequences were analyzed in the GenBank database and have been deposited in the GenBank database under accession numbers GU992376–GU992385.

3. Results and discussion

3.1. Electricity generation and potential drop

Following a short lag period (~60 h) after inoculation, voltage from all six reactors increased quickly and reached steady state within 4 days (continuous voltage data not shown). The first reactor was sacrificed 3 days after inoculation, when the voltage was in its linear increase stage. The subsequent samples were chosen when voltages were stable at around 480 mV (118 mW/m^2 at an external resistance of 1000 Ω). All the reactors showed comparable voltage profiles throughout the experiment, and reactor selection was performed randomly. Even though the voltage after 3 days had reached 80% percent of the stable value (380 mV vs. 480 mV), it showed a very low polarization performance (Fig. 1A). From 3 days to 1 week, the electrochemical performance of the reactor improved significantly and was stable through week 2. In week 3, the open circuit voltage (OCV) of the sample reactor had dropped by 120 mV, and this was also observed in both week 6 reactors. The corresponding power densities of the parallel replicate systems achieved a maximum at week 2 of 197 mW/m^2 and then declined to 135 mW/m^2 on weeks 3 and 6 (Fig. 1B).

In an attempt to correlate the OCV drop to the power density drop for the MFCs operated for 3 or more weeks, a power density correction line was drawn as a function of current density based on the OCV drop. At the current density of 0.5 A/m^2, which was near the peak of the power density curves, the power density difference between week 2 and weeks 3 and 6 was approximately 62 mW/m^2, which correlates well with the power density correction of 60 mW/m^2 associated with the decreased OCV beyond 3 weeks of operation. Analysis of the open circuit potential (OCP) of individual electrodes showed that the reactor cathode potential dropped ~100 mV (from 260 mV to 160 mV) between weeks 2 and 3, while the anode potential increased only slightly between weeks 2 and 3 from −484 to −472 mV. Therefore, the change of the cathode OCP was the main reason for the decrease of OCV and power density. Although it is not clear why the cathode OCP drop was sudden between weeks 2 and 3 and did not worsen beyond 3 weeks, it can be related to a mixed potential effect caused by biofilm growth on the cathode, with bacteria-induced electrochemical processes reducing the thermodynamic potential of the cathode (Bard and Faulkner, 2000). Because the cathode was exposed to air, the platinum side of the cathode was gradually covered with thick yellowish biofilm (data not shown). This mixed-culture biofilm on the cathode may have accepted electrons from the MFC circuit and respired oxygen as electron acceptor, thus inducing a different cathode potential from the virgin platinum cathode.

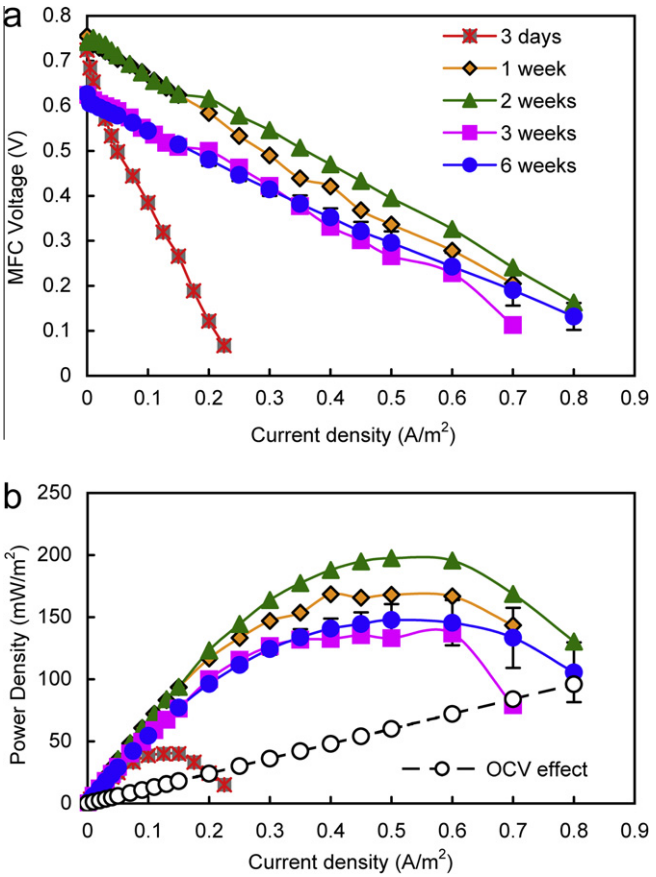

Fig. 1. Polarization curves (a) and power density curves (b) of MFCs operated for different durations. Dashed line shows the OCV correction between 2 and 6 weeks.

Other factors that may cause cathode potential reduction include cation concentration or pH gradients at the local cathode environment. On the other hand, since the anode potential remained nearly constant, the OCV drop observed was independent of the anode biofilm properties.

3.2. Charge transfer resistance variation

The EIS data were fitted with a Randle's type equivalent electrical circuit to obtain values for the anode and cathode charge transfer resistances (Ramasamy et al., 2008c). (A representative Nyquist plot for anode, cathode, and full-cell analysis is presented in Fig. S1, and Nyquist and Bode plots for the anode during biofilm development are presented in Fig. S2.) As the biofilm gradually developed on the anode, the anode charge transfer resistance at 25 mA/m^2 decreased from 9 kΩ-cm^2 on day 3 to 2.5 kΩ-cm^2 after 2 weeks, accompanied by an increase in peak power density, and remained stable thereafter (Fig. 2). In contrast, the cathode charge transfer resistance gradually increased throughout the experiment and tripled after 6 weeks, even though it was still over an order of magnitude lower than that of the anode. The value of anode impedance at 250 mA/m^2 was consistently around six times lower than at 25 mA/m^2, but the cathode impedance showed similar values at both current densities. The two week 6 reactors showed very similar results in terms of charge transfer resistances and open circuit potential. These trends were consistent, and comparable in magnitude, with our earlier study using two-chamber ferricyanide catholyte based MFCs and indicated a direct correlation between anode biofilm development and MFC performance (Ramasamy et al., 2008c).

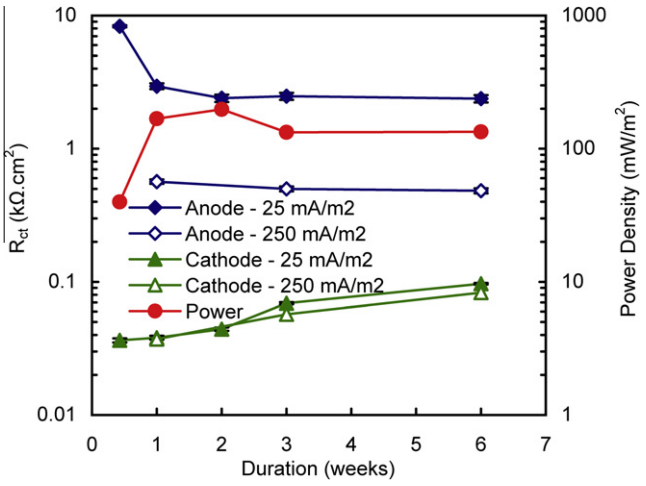

Fig. 2. Variation of the electrodes charge transfer resistances and maximum power density during the biofilm growth period.

3.3. Anode biofilm variation and the relation with electrochemical performance

After electrochemical analyses of each reactor, the anode biofilm was stained by LIVE/DEAD viability staining and visualized using a confocal laser scanning microscope. (Confocal images of anode biofilms are shown in Fig. S3.) As mentioned before, the reactor voltage at 1000 Ω had already reached 80% of the stable voltage after 3 days, but the system and anode electrochemical responses were quite weak. This is consistent with the anode biofilm development after 3 days, which was very scarce and comprised mostly of dispersed rod-shaped cells. Direct cell count showed a total cell density of 8.7×10^6 cells/cm^2 of the projected anode, 91% of which were viable (Fig. 3). DGGE screening of amplified 16S rRNA gene fragments from the anode community showed several prominent bands on day 3 (Fig. 4). The sequences from these bands were most phylogenetically related to the following isolates (Table 1): *Geobacter sulfurreducens* (band 1), *Pseudomonas panipatensis* strain Esp 1 (band 2), *Pseudomonas citronellolis* YS-8 (band 3), and *Clostridium aminovalericum* strain DSM 1283 (band 10). *G. sulfurreducens* is a well characterized acetate-utilizing exoelectrogen (Bond and Lovley, 2003), and it had a prominent DGGE band

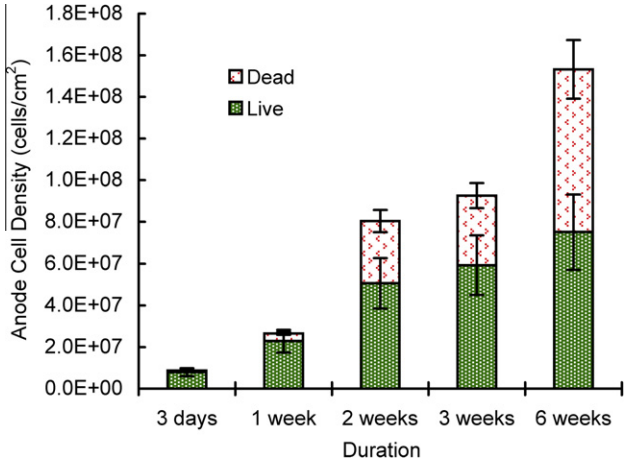

Fig. 3. Direct cell count of anode biofilm for different reactor operational durations. The green (bottom) part of each column represents live cells and the red (upper) part of each column represents dead cells. (For interpretation of the references to colour in this figure legend, the reader is referred to the web version of this article.)

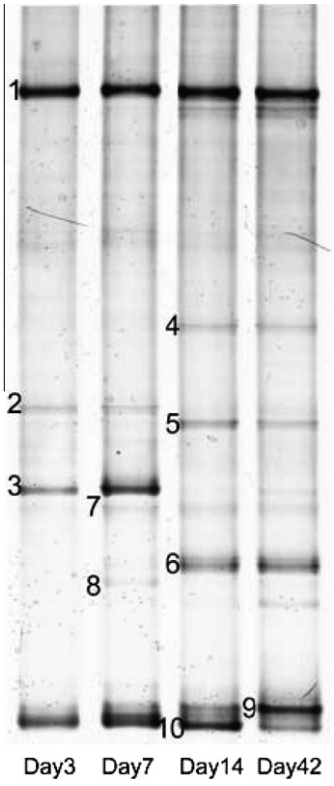

Fig. 4. 16S rRNA gene DGGE profiles of time-series anode biofilm samples, with numbering of prominent bands that were selected for sequencing.

Table 1
Phylogenetic identification of predominant 16S rRNA gene fragment DGGE bands.

Band	Closest cultivated isolate (accession number)	Similarity (%)
1	*Geobacter sulfurreducens* (GSU13928)	99
2	*Pseudomonas panipatensis* strain Esp1 (EF424401)	91
3	*Pseudomonas citronellolis* strain YS-8 (FJ462715)	99
4	*Erysipelotrichaceae* bacterium WH043 (AB298733)	91
5	Clostridium sp. FF08 (AB276319)	97
6	*Fusibacter* sp. VNs02 (FJ168472)	92
7	*Clostridium* sp. LTR1 (AF427155)	96
8	*Pseudomonas* sp. SZDN-2 (GU222443)	93
9	*Pseudomonas fluorescens* strain 2–79 (FJ652606)	100
10	*Clostridium aminovalericum* strain DSM 1283 (NR_029245)	97

throughout the 6 weeks of operation. The other three isolates are uncharacterized with respect to exoelectrogenesis. After 1 week, when the reactor voltage at 1000 Ω had stabilized, the microbial attachment had increased significantly. Even though the biofilm was still dispersed, the total cell density tripled to 2.7×10^7 cells/cm^2, and the ratio of live to total cells was approximately 85% (Fig. 3). The prominent DGGE bands did not change much from the 3 day profile, with the additional appearance of faint bands with sequences most related to the iron-reducing *Clostridium* sp. LTR1 (Scala et al., 2006) and *Pseudomonas* sp. SZDN-2 (bands 7 and 8, respectively).

Beginning from week 2, when the system had the highest peak power density, the anode biofilm was getting much denser and aggregates were observed on the carbon fiber surface. Most of the microorganisms were rod or sphere shaped, but small, filamentous structures were detected for the first time. The total cell density tripled again to 8×10^7 cells/cm^2, but the percentage of viable cells dropped to around 63% of the total cell count (Fig. 3). The

DGGE community profiling showed the emergence of sequences most similar to an *Erysipelotrichaceae* (band 4), the fumarate-reducing *Clostridium* sp. FF08 (Hattori and Matsui, 2008) (band 5), *Fusibacter* sp. VNs02 (band 6), and *Pseudomonas fluorescens* strain 2–79 (band 9), with the fading of bands 3 and 8 associated with *Pseudomonas* spp. The family *Erysipelotrichaceae* has only one accepted genus, *Erysipelothrix*, which includes aerobic and facultative members, some of which are known to produce long filaments (Dworkin et al., 2006). *Fusibacter* have been detected in other MFC studies (Rezaei et al., 2009; Xing et al., 2010), but their specific roles in the biofilm ecology are unknown. *P. fluorescens* strain 2–79 is a characterized producer of phenazines (Mavrodi et al., 2010), which have been shown in other studies to contribute to current production as mediators (Rabaey et al., 2005). After 6 weeks, filamentous microbes became the dominant morphology, forming large clusters around the intersections of carbon fibers. The density of total cells increased to 1.5×10^8 cells/cm^2, but the live cells only accounted for 48% of the total cell count (Fig. 3). There was an accumulation of dead cells, with a relatively small change in the viable cell count after week 2. Confocal pictures showed that live and dead cells were colocalized, with no clear viability stratification from the bottom to the surface of the biofilm. There was no appreciable change in the DGGE profile between weeks 2 and 6.

As the anode viable and total cell density increased, the morphology of the anode biofilm progressively developed from dispersed individual cells to tight aggregates, and from rod-shaped cells to a filament-dominant structure. Anode community shifts have been reported in other studies (Aelterman et al., 2006; Bond et al., 2002; Jung and Regan, 2007; Orloff et al., 2007; Xing et al., 2009), yet no mixed-culture time-course biofilm morphology and composition variation has been linked with electrochemical performance. *Rhizobiales* bacteria with filamentous appendages have been found dominant in cellulose-fed MFCs (Ishii et al., 2008), but no such structure has been reported in acetate-fed systems. Of the identified community members in this present study, only the *Erysipelotrichaceae*-like sequence is related to a known filament-forming bacterium.

It is unclear what selective pressures led to the enrichment of filamentous bacteria. These filamentous structures might simply have been more resistant to shear force during medium changes (Liu and Tay, 2002), but their accumulation did not appear to affect power production. The extracellular electron transfer capabilities of filamentous bacteria have not been reported. This community shift to filamentous bacteria during stable MFC operation has a potential implication in using MFCs for wastewater treatment. One of the main concerns of biofilm reactors is clogging, especially when the influent contains particles. While filamentous structures are known to be resistant to organic or hydraulic shock, they can also prompt clogging and slow down biofilm regeneration (Lin et al., 2004). Using an open-structure anode material like a carbon brush might alleviate clogging concerns (Logan et al., 2007).

While both the live and total cell counts increased over the six-week duration of operation, different accumulation trends were observed (Fig. 3). The viable cell density dominated in early biofilms but approached an asymptote after 2 weeks. In comparison, the dead cells accumulated linearly with time, resulting in a continuous decrease of the viable fraction. Since viable cells serve as the active biocatalysts and transfer electrons to the anode, the increase of viable cells would reduce the anode charge transfer resistance. This relationship was observed (Figs. 2 and 3), as anode charge transfer resistance decreased until week 2, when viable cell density began to stabilize. Further biofilm development did not increase power production, suggesting a potential threshold of live cells existed in this system that is sufficient for maximum power output. Though other constraints may limit system performance as well, this finding indicates that stabilized live biofilm density can be one determining factor of system performance.

4. Conclusions

Using single-chamber air–cathode MFCs, this study showed that a stable voltage output under a constant external resistance may indicate steady state of electrochemical performance but not necessarily of the anode biofilm. The closed-circuit voltage stabilized within one week and maintained repeatable profiles with subsequent batch cycles, but the anode biofilm gradually developed during the six-week operation as observed in cell counts, biofilm morphology, and community structure. The results also showed a direct relationship between live cell density and electrochemical reaction kinetics. This link offers insights into the constraints of anode biofilm on MFC power outputs as well as design optimization.

Acknowledgement

This research was supported by National Science Foundation Grant CBET-0834033, a seed grant from the MRSEC program at Penn State (National Science Foundation Grant DMR-0820404), and Award KUS-I1-003-13 from the King Abdullah University of Science and Technology (KAUST).

Appendix A. Supplementary data

Supplementary data associated with this article can be found, in the online version, at doi:10.1016/j.biortech.2010.06.003.

References

Aelterman, P., Rabaey, K., Pham, H.T., Boon, N., Verstraete, W., 2006. Continuous electricity generation at high voltages and currents using stacked microbial fuel cells. Environ. Sci. Technol. 40, 3388–3394.

Bard, A., Faulkner, L., 2000. Electrochemical Methods: Fundamentals and Applications, second ed. John Wiley and Sons, New Jersey.

Bassam, B.J., Caetano-Anolles, G., Gresshoff, P.M., 1991. Fast and sensitive silver staining of DNA in polyacrylamide gels. Anal. Biochem. 196, 80–83.

Bond, D.R., Lovley, D.R., 2003. Electricity production by *Geobacter sulfurreducens* attached to electrodes. Appl. Environ. Microbiol. 69, 1548–1555.

Bond, D.R., Holmes, D.E., Tender, L.M., Lovley, D.R., 2002. Electrode-reducing microorganisms that harvest energy from marine sediments. Science 295, 483–485.

Cheng, S., Liu, H., Logan, B.E., 2006. Increased performance of single-chamber microbial fuel cells using an improved cathode structure. Electrochem. Commun. 8, 489–494.

Dworkin, M., Falkow, S., Rosenberg, E., Schleifer, K.-H., Stackebrandt, E., 2006. The Prokaryotes: A Handbook on the Biology of Bacteria, third ed. Springer.

Gorby, Y.A., Yanina, S., McLean, J.S., Rosso, K.M., Moyles, D., Dohnalkova, A., Beveridge, T.J., Chang, I.S., Kim, B.H., Kim, K.S., Culley, D.E., Reed, S.B., Romine, M.F., Saffarini, D.A., Hill, E.A., Shi, L., Elias, D.A., Kennedy, D.W., Pinchuk, G., Watanabe, K., Ishii, S., Logan, B., Nealson, K.H., Fredrickson, J.K., 2006. Electrically conductive bacterial nanowires produced by *Shewanella oneidensis* MR-1 and other microorganisms. PNAS 103, 11358–11363.

Hattori, K., Matsui, H., 2008. Diversity of fumarate reducing bacteria in the bovine rumen revealed by culture dependent and independent approaches. Res. Microbiol. 160, 107–116.

He, Z., Mansfeld, F., 2009. Exploring the use of electrochemical impedance spectroscopy (EIS) in microbial fuel cell studies. EnergyEnviron. Sci. 2, 215–219.

Ishii, S., Shimoyama, T., Hotta, Y., Watanabe, K., 2008. Characterization of a filamentous biofilm community established in a cellulose-fed microbial fuel cell. BMC Microbiol. 8, 6.

Jung, S., Regan, J.M., 2007. Comparison of anode bacterial communities and performance in microbial fuel cells with different electron donors. Appl. Microbiol. Biotechnol. 77, 393–402.

Kim, J., Jia, H.F., Wang, P., 2006. Challenges in biocatalysis for enzyme-based biofuel cells. Biotechnol. Adv. 24, 296–308.

Lin, H., Ong, S.L., Ng, W.J., Khan, E., 2004. Monitoring of bacterial morphology for controlling filamentous overgrowth in an ultracompact biofilm reactor. Water Environ. Res. 76, 413–424.

Liu, Y., Tay, J.H., 2002. The essential role of hydrodynamic shear force in the formation of biofilm and granular sludge. Water Res. 36, 1653–1665.

Logan, B.E., Regan, J.M., 2006. Electricity-producing bacterial communities in microbial fuel cells. Trends Microbiol. 14, 512–518.
Logan, B., Hamelers, B., Rozendal, R., Schröder, U., Keller, J., Freguia, S., Aelterman, P., Verstraete, W., Rabaey, K., 2006. Microbial fuel cells: methodology and technology. Environ. Sci. Technol. 40, 5181–5192.
Logan, B., Cheng, S., Watson, V., Estadt, G., 2007. Graphite fiber brush anodes for increased power production in air-cathode microbial fuel cells. Environ. Sci. Technol. 41, 3341–3346.
Manohar, A.K., Bretschger, O., Nealson, K.H., Mansfeld, F., 2008. The polarization behavior of the anode in a microbial fuel cell. Electrochim. Acta 53, 3508–3513.
Mavrodi, D.V., Peever, T.L., Mavrodi, O.V., Parejko, J.A., Raaijmakers, J.M., Lemanceau, P., Mazurier, S., Heide, L., Blankenfeldt, W., Weller, D.M., Thomashow, L.S., 2010. Diversity and evolution of the phenazine biosynthesis pathway. Appl. Environ. Microbiol. 76, 866–879.
Mench, M., 2008. Fuel Cell Engines. John Wiley and Sons, New Jersey.
Orloff, A., Johnson, J., Nevin, K.P., Lovley, D.R., 2007. Influence of anode potential on microbial communities colonizing the anodes of microbial fuel cells. American Society for Microbiology 107th General Meeting, Toronto, Canada.
Rabaey, K., Boon, N., Hofte, M., Verstraete, W., 2005. Microbial phenazine production enhances electron transfer in biofuel cells. Environ. Sci. Technol. 39, 3401–3408.
Ramasamy, R.P., Cloud, S.R., Ren, Z., Regan, J., Mench, M., 2008a. Effect of biofilm properties on the electrochemical performance of microbial fuel cells. ECS Trans. 13, 11–17.
Ramasamy, R.P., Ren, Z., Mench, M., Regan, J.M., 2008b. Microbial fuel cells for waste water treatment. ECS Trans. 11, 115–125.
Ramasamy, R.P., Ren, Z., Mench, M.M., Regan, J.M., 2008c. Impact of initial biofilm growth on anode impedance in microbial fuel cells. Biotechnol. Bioeng. 101, 101–108.
Reguera, G., McCarthy, K.D., Mehta, T., Nicoll, J.S., Tuominen, M.T., Lovley, D.R., 2005. Extracellular electron transfer via microbial nanowires. Nature 435, 1098–1101.
Ren, N., Xing, D., Rittmann, B.E., Zhao, L., Xie, T., Zhao, X., 2007a. Microbial community structure of ethanol type fermentation in bio-hydrogen production. Environ. Microbiol. 9, 1112–1125.
Ren, Z., Ward, T.E., Regan, J.M., 2007b. Electricity production from cellulose in a microbial fuel cell using a defined binary culture. Environ. Sci. Technol. 41, 4781–4786.
Ren, Z., Steinberg, L.M., Regan, J.M., 2008. Electricity production and microbial biofilm characterization in cellulose-fed microbial fuel cells. Water Sci. Technol. 58, 617–622.
Rezaei, F., Richard, T.L., Logan, B.E., 2009. Analysis of chitin particle size on maximum power generation, power longevity, and Coulombic efficiency in solid-substrate microbial fuel cells. Biosens. Bioelectron. 25, 105–111.
Scala, D.J., Hacherl, E.L., Cowan, R., Young, L.Y., Kosson, D.S., 2006. Characterization of Fe(III)-reducing enrichment cultures and isolation of Fe(III)-reducing bacteria from the Savannah River site, South Carolina. Res. Microbiol. 157, 772–783.
Xing, D., Cheng, S., Regan, J.M., Logan, B.E., 2009. Change in microbial communities in acetate- and glucose-fed microbial fuel cells in the presence of light. Biosens. Bioelectron. 25, 105–111.
Xing, D., Cheng, S., Logan, B.E., Regan, J.M., 2010. Isolation of the exoelectrogenic denitrifying bacterium *Comamonas denitrificans* based on dilution-to-extinction of the microbial community. Appl. Microbiol. Biotechnol. 85, 1575–1587.